Turbulent Scattering Spectra of Electron Density Fluctuations in Mach 16 Projectile Wakes

JAY FOX* AND HARALD RUNGALDIER†
TRW Systems Group, Redondo Beach, Calif.

The popular underdense scattering spectrum that was used by Salpeter and Treiman (1964) is compared for the first time with experimental measurements. The form of the spectrum is $F(K\Lambda) = 15.5\Lambda^3(1+K^2\Lambda^2)^{-11/6}$, where Λ is the turbulent scale and K is the electron density spectrum wavenumber. (K is twice the radar wavenumber in backscatter calculations.) Direct measurements of the three-dimensional spectrum in turbulent Mach 16 wakes behind sphere projectiles are obtained with fine-wire electron-collection probes operating in a free-molecule electron-saturation mode. The power-law slopes of the experimental spectrum are always steeper than the $-\frac{11}{3}$ slope of the prediction, which is consistent with the low Reynolds number character of these high Mach number experiments. When compared with the prediction, the experimental spectrum varies from +3 db to −8 db. A zone of high dissipation spectra is found near breakthrough where the probes were 25% off-axis. Similar results are found in Mach 9 spectra but not in Mach 6 spectra, the latter being farther off-axis.

Nomenclature

A = area
C_D = drag coefficient
D = diameter of projectile or wake
D_w = diameter of wire
e = charge of an electron
E = 3-dimensional spectrum
f = frequency, Hz
F = normalized 3-dimensional spectrum
I = electron collection current [Eqs. (1) and (2)]
k = Boltzmann constant
K = wavenumber in space
M = Mach number of projectile flow
M_e = mass of electron
n_e = electron density
n_e' = rms electron density
P = power spectrum
t = time or lag time
T = temperature or time
V = voltage or wake velocity
V_B = projectile velocity
X = axial distance behind projectile
Y = radial distance from projectile axis
γ = specific heat ratio
θ = time correlation integral scale
λ = mean free path
λ_D = Debye length
Λ = space correlation length scale

Subscripts

F = turbulent front or edge
FW = far wake trend of turbulent front
I = inviscid wake edge
P = probe

Introduction

A CONTINUING need for turbulent scattering information on hypersonic wakes has been shown by recent research activity.[1] Experimental spectrum comparisons with theoretical scattering models have been lacking, however. The capability of the fine-wire electrostatic probe to measure electron density directly in the electron-collecting mode has been used in this study of Mach 16 sphere wakes to obtain experimental scattering spectrum in a three-dimensional isotropic form. These local probe measurements have a superior fundamental appeal when compared with earlier volume-averaged measurements[2,3] and later ion-collecting electrostatic probes.[4,5] For comparison with a local scattering model, the volume-averaged measurements are the grossest possible comparison. The ion-collecting continuum probes unfortunately produce data that are inextricably intertwined with temperature and velocity; they cannot give instantaneous local electron density. Progress on direct measurements of electron density is reported in Ref. 6.

Theories of underdense scattering have been reviewed by Tatarski.[7] The microwave single scattering (Born approximation) theory, as described in Salpeter and Treiman,[8] states that the backscatter cross section is composed of a volume integral of the electron density fluctuation times the spectrum function of the electron density fluctuations

$$F(K,\Lambda) = 15.5\Lambda^3(1+K^2\Lambda^2)^{-11/6} \quad (1)$$

together with certain known constants. Although fluctuation measurements have been taken with various ion probes[4,5] and other probes,[9-12] the basic comparison of direct measurements of electron density fluctuation spectra with the popular model of Ref. 8 has not been accomplished. For the first time, these measurements are formulated into a three-dimensional spectrum in this report.

Previous Mach 9 measurements[12] probed the low Mach number limit of ionized wakes. Krypton gas was used to provide the high degree of ionization in the shock layer ahead of the projectile and in the wake. Ideal gas conditions are closely approximated under these conditions compared to airflow conditions where dissociation, vibration, and rotation play such an important role in absorbing molecular energy. The high stagnation temperature in krypton deviated somewhat from ideal gas conditions mainly due to ionization energy and trace contaminants of air.

Experimental Methods

Greater interest in turbulent scattering information can be found for the conditions of the present experiment at Mach 16. Much higher temperatures are encountered at this Mach number and significant energy is taken up by ionization. Emission from

Presented as Paper 72-673 at the AIAA 5th Fluid and Plasma Dynamics Conference, Boston, Mass., June 26–28, 1972; submitted June 28, 1972; revision received April 5, 1973. This work was supported by ARPA/SAMSO under contract F04701-71-C-0040.

Index categories: Jets, Wakes, and Viscid-Inviscid Flow Interactions; Plasma Dynamics and MHD; Reactive Flows.

* Staff Engineer, Re-entry Physics Department. Member AIAA.

† Member of the Technical Staff, Engineering Technology Department. Associate Member AIAA.

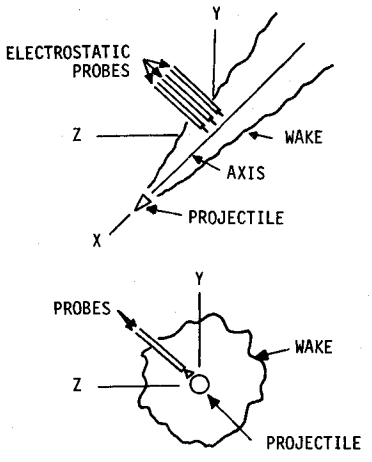

Fig. 1 Configuration of the ballistic range experiment.

PROJECTILE	HALF-INCH SPHERE
MACH NO.	16.5
GAS	KRYPTON (γ = 1.67)
PRESSURE	25 TORR
NO. OF SHOTS	7

the stagnation point region is encountered; shadowgraphs are difficult to make at this Mach number, whereas they are easy at Mach 9. Longer electron wakes are obtained at Mach 16 with higher initial levels. Microwave measurements showed electron density levels above 10^{12} cm^3 for the first 300 X/D, where lower levels were obtained at Mach 9 (Ref. 12).

The probe and projectile arrangement shown in Fig. 1 is similar to the previous experiments at Mach 6 and 9.[9-12] A new light-gas launcher was used to obtain 12 kfps velocity for the $\frac{1}{2}$-in. aluminum spheres; they were copper plated to 0.004-in. thickness. Other experimental results[2] showed no ablation for this condition at an equivalent Reynolds number. It should be noted that the effect of the heavy krypton gas is to give about twice the Reynolds number as compared with air.

At 25 torr of krypton, the microwave measurements showed transition occurring within a few diameters behind the body. The flight paths were close to the probes; the axis-to-probe distance averaged one projectile diameter and varied between 0.8 and 1.9. At this location, the probes are immersed by the growing turbulent wake after 40 diameters of projectile travel, as will be shown later by the Lees-Hromas calculations.

The electron-collection wires on the probes were 0.0001-in.-diam tungsten with a platinum 5-μin. coating. The classical collisionless theory with orbit-motion limiting[13] applied under these conditions. It should be noted that the survival of the fine wires depended in part on the short duration of the experiment, perhaps explaining the small amount of comparable data.

As indicated in the previous work,[12] the current collected at high positive bias [or $(eV)/(kT) \gg 1$] produced the limiting case from the theory; that is, the current I was proportional to the electron density n_e and independent of temperature T. The resulting relation is

$$I = eAn_e(2eV/\pi^2 M_e)^{1/2} \qquad (2)$$

A positive 10 v bias kept the possible 1 v plasma potential variations from causing more than 5% data variations. Wake conditions at the probe were typically 1500°K, 25 torr of krypton and n_e about 10^{11}/cm^3, which gave validity to the collisionless collection theory. In fact, $\lambda/D_w = 10$ and $\lambda_D/D_w = 3$, whereas sheath diameters were $\frac{1}{10}$ of the wire length. References 14 and 5 show that Eq. (2) is valid for fluctuations as well, thus providing the means of calculating electron density fluctuations directly from electron collection current fluctuations.

Exposed collection wire length was 0.025 in. on each probe, and about 100 in. of ground wire was provided to keep the plasma within 1 v of ground. On one occasion, the ground wires were destroyed without affecting the collection wires; the effect of the rising plasma potential was clearly seen as a declining collection current. The absence of that problem on the good launchings was also recognizable.

Each collection wire was supported on two posts 0.10 in. apart[16] but it was connected electrically to just one. Current-to-voltage transducers at the base of the probes provided the output data that was tape recorded. Overlapping sensitivities on the two tape recorder channels for each probe were provided in order to maximize the signal-to-noise for the data along the decaying electron-density wake. The high frequency data on this experiment required a d.c. to 500 KHz bandwidth tape recorder. Digitizing at the rate of 380,000 samples/sec on each probe channel provided data analysis frequencies up to 190 KHz on the digital computer. Segments of the data from $\frac{1}{4}$ msec to 2 msec long were analyzed to produce the spectra.

One-Dimensional Spectra

The one-dimensional spectra were calculated from the Fourier cosine-transformed correlations using 20% maximum lag in each data segment; this procedure is the same as that used before.[12] The resulting raw spectra were resubmitted to the digital computer on a separate processing program which subtracted out the noise as a first step. In all cases the noise was dominated by the tape recorder so that an average noise spectrum could be calculated from the record before the shot. This noise spectrum was subtracted from each data spectrum and the resulting "clean" spectrum was then normalized by its covariance or mean square power. The individual spectra with sufficient signal-to-noise ratio were averaged. Various inspections and integral checks were made of the averaging process to make sure the Fourier transform properties of the spectra were maintained on the average spectrum.

The resulting average one-dimensional spectra of electron density fluctuations are shown in a normalized form in Fig. 2. The value of the spectrum at zero frequency $P(0)$ is taken as the normalizing value. The abscissa is the normalized wave-number product $K\Lambda$ where K is the spatial wavenumber of the fluctuations and Λ is the space integral scale of the fluctuations. Neither of these quantities needs to be known individually because they both convert from the corresponding time values through "Taylor's Hypothesis," that is, $K = 2\pi f/V$ and $\Lambda = \theta V$ where V is the local average velocity, f is frequency, and θ is the integral of the autocorrelation function; additionally, the velocity V does not have to be measured.

Figure 2 is a composite graph of all the one-dimensional

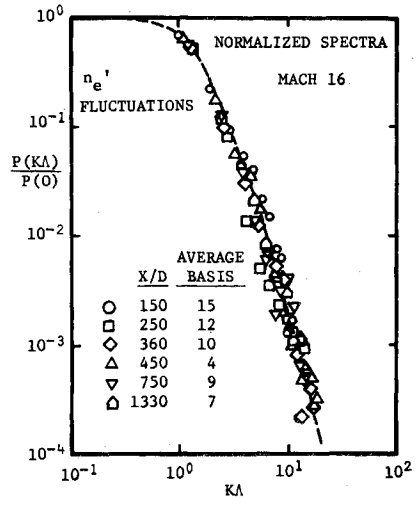

Fig. 2 Normalized one-dimensional spectra of electron density fluctuations in Mach 16 sphere wakes.

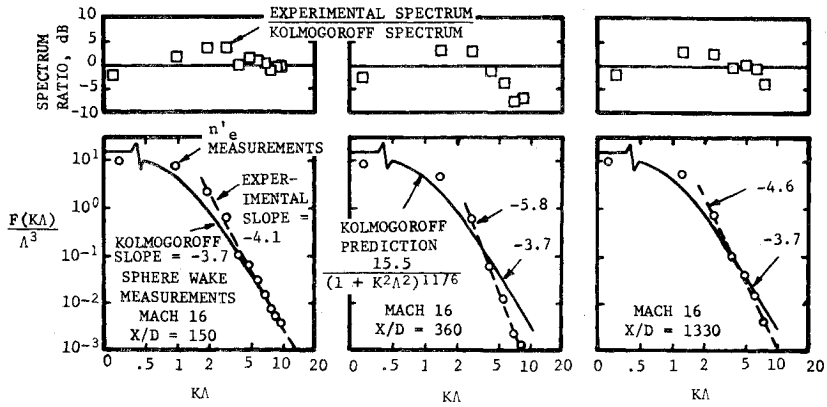

Fig. 3 Three-dimensional spectrum of electron density fluctuation measurements in Mach 16 sphere wakes: a) $X/D = 150$, b) $X/D = 360$, c) $X/D = 1330$. The upper part of the picture is the ratio of experimental spectrum to predicted spectrum.

spectra calculated at six locations from $X/D = 150$ to 1330, where the center of the data interval is taken as the nominal location. The average basis, that is, the number of individual spectra contributing to the average spectrum, ranged from 15 to 4 according to the signal-to-noise properties at that location. For the seven shots with data reduction, three probes were available making a maximum possible basis of 21. The low X/D locations had the greatest average basis, as a rule.

This normalization in Fig. 2 shows the greatest collapsing of the data about the nominal line at low $K\Lambda$. (The line is intended as a guide for visualization only.) The high wavenumber values vary significantly from the line according to the local dissipation properties. Further examination of these features will be made in the following section.

The format shown in Fig. 2 is similar to the final figure of the previous measurements at Mach 9 (Ref. 12). In order to make a more meaningful comparison with scattering theory, the three-dimensional isotropic spectra of the data were calculated.

Three-Dimensional Spectra

At the six X/D locations, the one-dimensional spectra of Fig. 2 were transformed into the correlation function and then retransformed using a three-dimensional Fourier transform. The retransform assumes isotropy or spherical symmetry of the correlation function in the three directions.[17] In particular, the three dimensional spectrum $E(f)$ is

$$E(f) = (1/2\pi^2)\int t^2(\sin 2\pi ft/2\pi ft)R(t)\,dt \qquad (3)$$

where $R(t)$ is the autocovariance or correlation function and t is the lag time. Isotropy is a well-known property of turbulent flows in the fine scale fluctuations that make up most of the spectrum.

Particular examples of three-dimensional spectra are shown in Figure 3 for the Mach 16 wake data. The lower part of the figure is the spectra of the electron density fluctuations n_e' which are normalized by Λ^3, again through the properties of Taylor's hypothesis. The spectrum F is E so normalized that[8]

$$\int_0^\infty F(K)K^2\,dK = 2\pi^2 \qquad (4)$$

The previously mentioned prediction used by Salpeter and Treiman[8] is also shown in Fig. 3 where it is called "Kolmogoroff prediction." The Kolmogoroff power law slope of $-\frac{11}{3}$ is the high wavenumber limit of the prediction.

It is noteworthy that the experimental power law slope is readily determined in the three examples of Fig. 3 as well as in all of the other calculated spectra. Further, the experimental slope is always steeper than the prediction, a fact which held true for all of the scattering spectra that were calculated. Higher experimental spectra than the prediction were obtained around $K\Lambda = 2$ and lower experimental values than the predicted values held at higher wavenumbers.

The relative magnitudes of experimental and predicted spectra are shown in the upper part of Fig. 3, where the spectrum ratio is shown as decibels above or below the prediction. This display form makes the comparison easier to visualize and make possible a summary comparison on a single figure.

Figure 4 shows these spectrum ratios for most of the calculated spectra at Mach 16. The features of high ratio at low $K\Lambda$ and low ratio at high $K\Lambda$ is clearly shown. In order to make the comparison of spectra more compact, certain features of these spectrum ratios were identified. As shown at $X/D = 360$ in Fig. 4, the maximum spectrum ratio and the minimum spectrum ratio were identified as experimental values above or below the prediction.

It may be seen in Fig. 4 that there is a different character to

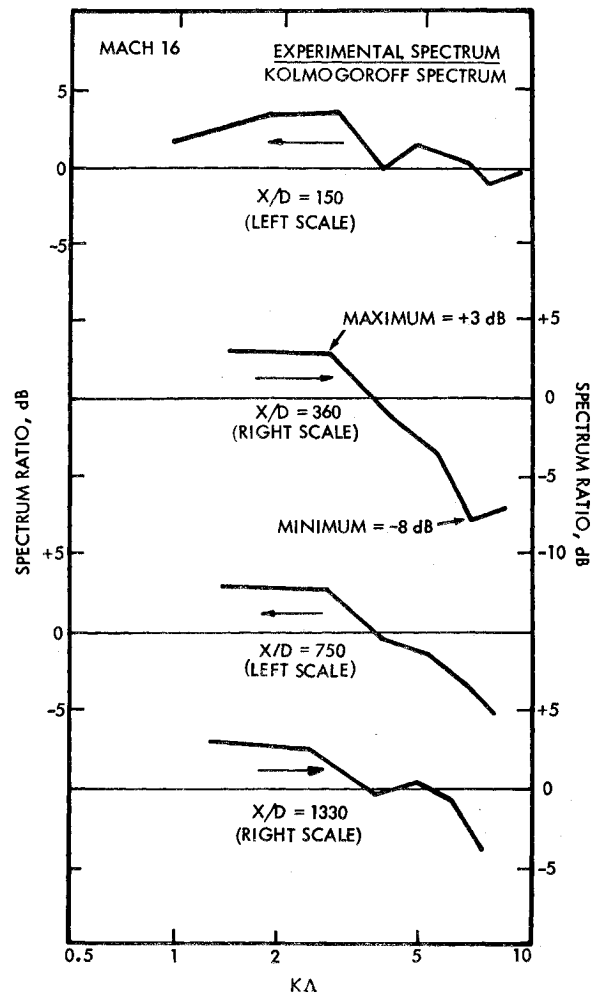

Fig. 4 Ratio of experimental-to-predicted spectrum of electron density fluctuation measurements in sphere wake at Mach 16.

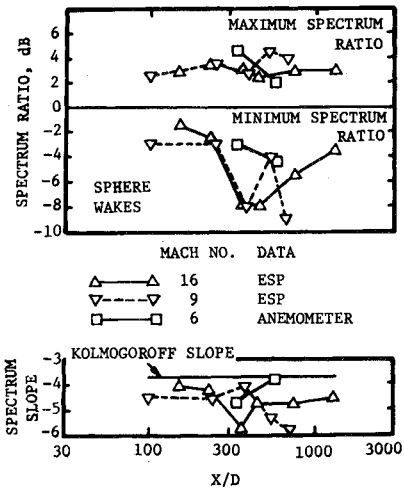

Fig. 5 Maximum and minimum spectrum ratio, and slope of three-dimensional spectrum in sphere wake measurements at Mach 16, 9, and 6.

the spectrum at $X/D = 360$ as compared to the lower or higher X/D. In particular, the spectrum ratio has a steeper slope and falls to a lower minimum value than those at other X/D. This behavior is associated with a greater dissipation at high wavenumbers as compared with the energy-containing eddies at low wavenumber.

Mach Number Effects

Three-dimensional spectra were calculated from the previously measured sphere wake spectra at Mach 6 and 9. These spectra were measured with anemometers and electrostatic probes, respectively, but $\frac{1}{2}$-in. sphere projectiles were used throughout. Maximum and minimum spectrum ratios as well as the power-law slopes were extracted from each spectrum. The combined display of these features from Mach number spectra is shown in Fig. 5. The maximum spectrum ratio is shown to be as much as 5 db, that is, the experimental spectrum is measured to be as much as a factor of 3 above the prediction. Likewise, minimum spectrum ratios are as much as -9 db, or experimental spectrum values a factor of 8 smaller than the prediction. Experimental power-law slopes are shown to be approaching -6 in steepness compared with -3.7 slope which is the Kolmogoroff slope.

The Kolmogoroff slope is the theoretical limit of a shallow slope at high turbulence Reynolds number. The region of the spectrum that transfers the energy from the large eddies to the small eddies is stretched out under high Reynolds number conditions. This effect gives a long spectral region between the energy-containing eddies at low wavenumber and the viscous-dissipating eddies at high wavenumber. In between, there is a zone where energy is transferred across the spectrum from the large eddies to the small eddies. Kolmogoroff deduced the slope for this transfer region under the extreme limiting conditions of high turbulence Reynolds number.[17]

Under lowering turbulence Reynolds number conditions the dissipation occurs in larger and larger eddies until the whole spectrum can be dissipating everywhere; the slope is not the limiting $-\frac{11}{3}$ and it may not be a single slope but rather a curve. It is notable that the slope can be obtained from the three-dimensional spectra but that it rarely approaches the shallow (Kolmogoroff) limit, as shown in Fig. 5.

A complicating effect of Mach number on the spectrum changes the consideration of the turbulence Reynolds number. At low Mach number, the same turbulence Reynolds number as obtained in Fig. 5 produces a significant length of Kolmogoroff slope.[18] Under high Mach number conditions, the wake axis velocity is the high velocity that is taken as the characteristic velocity. This high velocity is accompanied by a high temperature and a low density. The axis properties of density and viscosity, which are taken into account in the above-mentioned Reynolds-number comparisons with low speed flow,[18] provide a significant effect on the calculated turbulence Reynolds number. In particular, they provide a factor of $\frac{1}{10}$ when compared with external properties.

In appearance, the spectra measured here are similar to lower Reynolds number spectra measured for incompressible flow conditions. The cause of this effect may be related to a loss of "mixing power" when the high velocity portion of the flow is at a low density. The spectral transfer effect may be changed or inhibited compared with that from the limiting Kolmogoroff conditions of high Reynolds number with incompressibility. At large X/D, the turbulence Reynolds number decreases as $(X/D)^{-1/3}$ so that the opportunities for Kolmogoroff spectra likewise decrease rapidly with X/D.

In Fig. 5, there can be observed at Mach 16 evidences of greater dissipation at $X/D = 360$ to 450. There are the steeper slopes at that range of X/D than at lesser or greater X/D, and there are the low spectrum ratio minimums. Similar evidences are found at Mach 9 although at a somewhat larger X/D range, specifically, $X/D = 525$ to 660. Mach 6 spectral data is more limited and doesn't show these features. In order to relate these factors to other characteristics of the wake, wake predictions using the Lees-Hromas method were calculated. They are discussed in the next section.

Off-Axis Location

An existing computer program developed from the Lees-Hromas theory[19-22] was used to calculate the mean wake properties for the range of conditions encountered in the ballistic range experiments. Drag coefficients were near 0.9, varying somewhat according to ballistic range data.[23]

The primary motivation for calculating the mean wake predictions is to locate the probe spectrum measurements with respect to the wake edge or front. For the case of the Mach 16.5 measurements, the wake edge prediction is shown in Fig. 6. Probe location Y_P is shown to be one projectile diameter off-axis, on the average. The far wake trend Y_{FW} and the front radius Y_F are also shown as well as the inviscid wake radius Y_I. The "bulge" of Y_F over Y_{FW} is shown to occur at about the intersection of the inviscid wake radius Y_F. At this point all of the high enthalpy flow in the inviscid wake has been swallowed by the turbulent core flow. Cooling of the wake follows with increasing X/D.

It should be noted that the definition of the inviscid wake edge is somewhat arbitrary because the shape of the inviscid wake is a gaussian shape with the edge being asymptotic in nature. This feature is similar to a boundary-layer edge, and a similar problem of defining the edge exists. The definition used here was a value of 1% enthalpy increase, which was the point where the digital computer was told the edge existed for practical

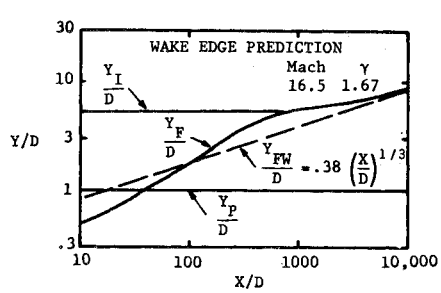

Fig. 6 Prediction of sphere wake edge including inviscid wake edge and experimental probe location for Mach 16 experiment conditions. Lees-Hromas calculation method.

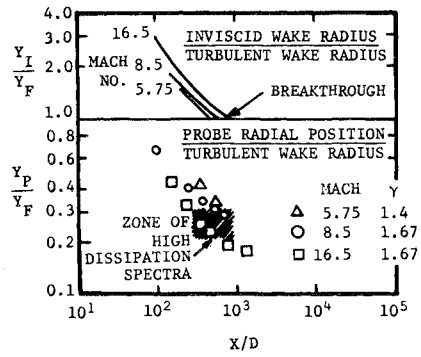

Fig. 7 Comparison of inviscid wake radius and probe radial position with the turbulent wake radius obtained by the Lees-Hromas calculation method. Zone of high dissipation spectra refers to characteristics shown in Fig. 5.

purposes. Comparisons with data are equally ambiguous because the edge is defined by some sensitivity level of an instrument system. Holographic interferometer data at Mach 5.75 agree with this definition when due regard for random variations is taken.[24] In particular, the schlieren-contrast line representing maximum integrated density derivative[25] is located somewhat closer to the wake axis. This location will take on added significance in the next section when breakthrough is discussed.

Dissipation-Spectra Zone

In Fig. 7, the location of the probe spectra measurements is shown as a fraction of the turbulent wake radius Y_F; all Mach numbers are shown. The upper part of Fig. 7 shows the inviscid wake radius Y_I on the same basis, that is, as a ratio to the turbulent front radius Y_F. Breakthrough is shown as the intersection of the inviscid wake radius with the growing turbulent front.

The zone of high dissipation spectra shown in Fig. 7 refers back to the features of the spectra that were summarized on Fig. 5. Specifically, the high dissipation characteristics are the low minimum spectrum ratio and the steep slope of the spectrum. (A low dissipation spectrum follows the Kolmogoroff prediction more closely and is characterized by a high turbulence Reynolds number.) The high dissipation spectra are shown in Fig. 7 to be located in a restricted zone of off-axis dimensions and axial locations, namely, Y_P/Y_F from 0.2 to 0.3 and X/D from 300 to 800. High dissipation was measured at Mach 16.5 and 8.5 but not at 5.75, so there may be a Mach number limitation as well.

The measurements of spectra at Mach 8.5 entered this zone at the end of the electron wake; oxygen attachment kept the electrostatic probes from measuring at greater X/D. At Mach 16.5, on the other hand, the measurements were made on both sides of this zone. In the measurements sequence with increasing X/D, lower dissipation spectra were obtained both before and after this middle zone.

There is some evidence that high dissipation is associated with the off-axis location of the measurement. In low-speed flow, sphere wake spectra were measured with high dissipation at an off-axis location.[18] The location was far enough off-axis so that the velocity fluctuations were only 3% of the axis value. Direct comparisons with the hypersonic measurements are tenuous at best. The physical argument for off-axis effects shows that the mixing occurs mostly around the maximum shear or velocity gradient. There is a diffusing effect that puts high turbulence material in both directions from the mixing zone, that is, toward the axis and away from it. The off-axis material tends to reside for a long time without much additional mixing and has a long time for dissipation. The axis material gets mixing from both sides and gets less time for dissipation.

In the Mach 16 flowfield, this line of argument would find difficulty in explaining the smaller dissipation at low X/D and large Y_P/Y_F. There would have to be a separate argument for this effect, such as the additional stimulation from the instabilities in the near wake that get transmitted in the acoustic mode. Ballistic-range schlieren photographs often show these irregularities.[26] Hypersonic near wake measurements[1] in wind tunnels show turbulent flow properties in electron measurements that extend to large off-axis locations in the inviscid wake compared to the turbulent core edge, but the mixing is restricted to the turbulent core. Acoustic mode propagation makes possible the off-axis irregularities in the steep electron density gradient that comprises the inviscid wake.

Breakthrough is a flow feature that occurs at about the X/D location where the high-dissipation zone was measured. The locations at Mach 5.75, 8.5, and 16.5 are shown to be $X/D = 500$, 600, and 900, respectively. These locations are greater than the usually accepted values because of the definition that was used here. The term breakthrough became popular in describing the breakthrough of the turbulent core beyond the schlieren-contrast width of an inviscid wake.[26] As mentioned previously, this width is narrower than the enthalpy profile width value, and it produces a smaller X/D value for breakthrough. For Mach 20 conditions in air, values for schlieren breakthrough as low as $X/D = 50$ have been found.

The possible importance of breakthrough to the dissipation zone should not depend on its detailed definition but rather on the fundamental physics of the flowfield. As can be seen in Fig. 6, the region near breakthrough has a rapid growth rate; the wake diameter increases rapidly in the power-law sense. There may be some reason to argue that the rapid growth takes place first in the energy-containing large eddies that reside at low wavenumber in the spectra. The large shear term or eddy diffusivity term is known[17] to engage the large eddies first and then they in turn energize the smaller eddies in the spectrum, as discussed in the Reynolds number discussion above. There may be reason to believe that the spectral transfer function is slower in this flowfield around breakthrough where the high-speed flow has such low density compared to the outside flow density.

Conclusions

Three-dimensional scattering spectra were calculated from new and existing data measured with electrostatic probes and anemometers; turbulent sphere wakes at Mach 16.5 for the new data and at Mach 8.5 and 5.75 for the existing data were the experimental flowfield. Mean wake calculations using the Lees-Hromas method showed the 25% off-axis location of high-dissipation spectra that occurred near breakthrough. The turbulence-Reynolds-number significance of spectral dissipation and transfer was discussed. Arguments for the significance of breakthrough and off-axis location were presented, but the evidence was not overweighing in either direction. When compared with the Kolmogoroff spectral prediction for high turbulence Reynolds number, the measured high dissipation spectra ranged from 5 db above the prediction at low wavenumber to 9 db below the prediction at high wavenumber when the data at all of the Mach numbers were considered. Clearly, the local zone in X/D and Y_P/Y_F shown in Fig. 7 that contains the high dissipation spectra can be taken as evidence of either point of view or as a combination of influences. The Mach 6 spectra being near breakthrough but with low dissipation tends to support Y_P/Y_F as the more dominant influence.

References

[1] Naidenko, G. N., Young, M. C., Merritt, G., and Wixon, N., "Experiment in the Near Wake of a Sphere in Hypersonic Flow. Vol. I," CAL UB2974-0-1, March 1971, Cornell Aeronautical Lab., Buffalo, N.Y.

[2] Kornegay, W., "Electron Density Decay in Wakes," *AIAA Journal*, Vol. 3, No. 10, Oct. 1965, pp. 1819–1823.

[3] Hayami, R. A. and Primich, R. I., "Wake Electron Density

Measurements Behind Hypersonic Spheres and Cones," AGARD Conference Proceedings No. 19 (Preprint), Fluid Physics of Hypersonic Wake Conference, Fort Collins, Colo., May 1967.

[4] Cantin, A., Emond, A., and Heckman, D., "Observations on Electrostatic Probe Behavior in Ionized Turbulent Gas Flows in Ballistic Ranges," *Proceedings of the International Congress on Instrumentation in Aerospace Facilities,* IEEE Publication 69-C-19-AES, May 1969, pp. 20–33.

[5] French, I. P., Arnold, T. E., and Hayami, R. A., "Ion and Electron Distributions in Nitrogen and Air Wakes Behind Hypersonic Spheres," AIAA Paper 70-87, New York, 1970.

[6] Staff of the Aerophysics Division, "Reentry Physics Research Program on Turbulent Wakes," DREV M-2122/71, June 1971, Defence Research Establishment, Valcartier, Quebec, Canada.

[7] Tatarski, V. I., *Wave Propagation in a Turbulent Medium,* McGraw-Hill, New York, 1961.

[8] Salpeter, E. E. and Treiman, S. B., "Backscatter of Electromagnetic Radiation from a Turbulent Plasma," *Journal of Geophysical Research,* Vol. 69, No. 5, March 1964, pp. 869–881.

[9] Fox, J., Webb, W. H., Jones, B. G., and Hammitt, A. G., "Hot-Wire Measurements of Wake Turbulence in a Ballistic Range," *AIAA Journal,* Vol. 5, No. 1, Jan. 1967, pp. 99–102.

[10] Fox, J., "Space Correlation Measurements in the Fluctuating Turbulent Wakes Behind Projectiles," *AIAA Journal,* Vol. 6, No. 2, Feb. 1968, pp. 233–238; also Rept. 07854-6021-R000, Feb. 1967, TRW Systems Group, Redondo Beach, Calif.

[11] Fox, J. and Rungaldier, H., "Anemometer Measurements of Velocity and Density in Projectile Wakes," *AIAA Journal,* Vol. 9, No. 2, Feb. 1971, pp. 270–276.

[12] Fox, J. and Rungaldier, H., "Electron Density Fluctuation Measurements in Projectile Wakes," *AIAA Journal,* Vol. 10, No. 6, June 1972, pp. 790–795.

[13] Langmuir, I. and Mott-Smith, H. M., "The Theory of Collectors in Gaseous Discharges," *Physical Review,* Vol. 28, 1926, p. 727.

[14] Demetriades, A. and Doughman, E. L., "Langmuir Probe Diagnosis of Turbulent Plasmas," *AIAA Journal,* Vol. 4, No. 3, March 1966, pp. 451–459.

[15] Peterson, E. W. and Talbot, L., "Langmuir Probe Response in a Turbulent Plasma," *AIAA Journal,* Vol. 8, No. 8, Aug. 1970, pp. 1391–1398.

[16] Sutton, G. W., "Use of Langmuir Probes for Hypersonic Turbulent Wakes," *AIAA Journal,* Vol. 7, No. 2, Feb. 1969, pp. 193–199.

[17] Hinze, J. O., *Turbulence,* McGraw-Hill, New York, 1959.

[18] Uberoi, M. S. and Freymuth, P., "Turbulent Energy Balance and Spectra of the Axisymmetric Wake," *The Physics of Fluids,* Vol. 13, No. 9, Sept. 1970, pp. 2205–2210.

[19] Lees, L. and Hromas, L. A., "Turbulent Diffusion in the Wake of a Blunt Body at Hypersonic Speeds," Rept. 6110-6005-MU000, July 1961, TRW Space Technology Lab., Redondo Beach, Calif.; also *Journal of the Aerospace Sciences,* Vol. 29, 1962, pp. 976–993.

[20] Webb, W. H. and Hromas, L. A., "Turbulent Diffusion of a Reacting Wake," *AIAA Journal,* Vol. 3, No. 5, May 1965, pp. 826–837.

[21] Hromas, L. A. and Lees, L., "Effect of Nose Bluntness on the Turbulent Hypersonic Wake," Rept. 6130-6259-KU000, Oct. 1962, TRW Space Technology Lab., Redondo Beach, Calif.

[22] Lees, L., "Hypersonic Wakes and Trails," ARS Paper 2662-62, 1962; also *AIAA Journal,* Vol. 2, No. 3, March 1964, pp. 417–428.

[23] Bailey, A. B., "Sphere Drag Measurements in an Aeroballistics Range at High Velocities and Low Reynolds Numbers," AEDC-TR-66-59, May 1966, Arnold Engineering Development Center, Arnold Air Force Station, Tenn.

[24] Witte, A. B., Fox, J., and Rungaldier, H., "Localized Measurements of Wake Density Fluctuations Using Pulsed Laser Holographic Interferometry," *AIAA Journal,* Vol. 10, No. 4, April 1972, pp. 481–487.

[25] Webb, W. H., "Comments on Schlieren Measurements of the Inviscid Hypersonic Wake of a Sphere," *AIAA Journal,* Vol. 6, No. 11, Nov. 1968, pp. 2239–2240.

[26] Wilson, L. N., "Far Wake Behavior of Hypersonic Spheres," *AIAA Journal,* Vol. 5, No. 7, July 1967, pp. 1238–1244.